Fully Automatic Left Ventricle Segmentation in Cardiac Cine MR Images Using Registration and Minimum Surfaces

Marie-Pierre Jolly

Siemens Corporate Research, Imaging and Visualization Department Princeton, NJ
marie-pierre.jolly@siemens.com

Abstract. This paper describes a fully automatic system to segment the left ventricle in all slices and all phases of a magnetic resonance cardiac cine study. After localizing the left ventricle blood pool using motion, thresholding and clustering, slices are segmented sequentially. For each slice, deformable registration is used to align all the phases, candidate contours are recovered in the average image using shortest paths, and a minimal surface is built to generate the final contours. The advantage of our method is that the resulting contours follow the edges in each phase and are consistent over time. As part of the MICCAI grand challenge on left ventricle segmentation, we demonstrate using 15 training datasets and 15 validation datasets that the results are very good with average errors around 2 mm and the method is ready for clinical routine.

1 Introduction

Cardiovascular disease is now the largest cause of death in the modern world and is an important health concern. Physicians use non invasive technologies such as magnetic resonance (MR) imaging to observe the behavior of the heart and more specifically the left ventricle (LV). This paper proposes a system to automatically segment the LV in all slices and all phases of a cardiac MR cine study.

An MR cine study consists of 4D (3D+T) data and the segmentation of all the images can be tackled in various ways. Some researchers have attempted 4D segmentation [1]. We believe however that this approach is not feasible, since it is very difficult to build a model that is general enough to cover all possible shapes and dynamics of the LV and a model-free approach would not be constrained enough. The opposite approach is to segment each image individually [2]. This results in little cohesion between images and unsmooth contours over time. An intermediate approach used very often is to segment the LV in one phase (ED for example) on all slices [3, 4]. This can be quite difficult however. When a model is used, it needs to be carefully trained for all possible LV shapes and all possible MR acquisition protocols. Conversely, image-based techniques tend to be ad-hoc. We have chosen instead to segment all phases in one slice and propagate the segmentation between slices. This method can take advantage of the strong temporal correlation between phases to segment individual slices. For temporal propagation, researchers have proposed

using a dynamic model of the LV [5, 6] while other methods incorporate a tracking component into the recovery [7, 8]. We use deformable registration to align all phases and generate an average image that is then segmented. We then use minimal surfaces to enforce consistency between phases which is the main strength of our method. Contours follow the edges of the image in each phase and are smooth over time. We also use deformable registration to propagate the segmentation between slices.

In the next section, we will describe the main steps of our method. For the MICCAI grand challenge on left ventricle segmentation, it was only necessary to segment the endocardium and epicardium at ED and the endocardium at ES to compute the ejection fraction (EF) and the myocardial mass, which are the main clinical measurements. However, since it is more difficult to segment individual images or even individual phases, and our method makes use of temporal consistency, we segmented all images in the datasets. This also allows to compute additional measures such as blood pool volume over time, peak ejection and filling rates, and myocardial thickening. In Section 3, we demonstrate the performance of the method on 30 MICCAI challenge datasets.

2 Left Ventricle Segmentation

The proposed algorithm is completely automatic. It is divided into the following steps: 1) Heart localization; 2) Left ventricle blood pool detection; 3) Polar space transformation; 4) Gray scale analysis; and 5) Segmentation of the individual slices, which comprises of deformable registration to align all the phases, contour candidates on the average temporal image and minimal surface segmentation of all phases. We will describe each of these steps in more details.

The detection of the heart and the localization of the LV blood pool are described in Jolly [9]. First, we compute the first harmonic of the temporal Fourier transform in each slice, and extract the pixels which have a strong response. The final region of interest (ROI) consists of the most consistent connected components in space.

Otsu's thresholding is applied within the ROI in each slice to extract blood pixels which are then grouped into 2D+T connected components (CC) characterized by their shape, temporal behavior, position, etc. Isoperimetric clustering [10] is used to group CCs between slices and form the LV blood pool. The graph for the isoperimetric clustering algorithm consists of nodes for the 2D+T CCs and edges between overlapping CCs in neighboring slices. This process does not generate a blood pool region on all slices, nor does it handle the papillary muscles correctly in the blood pool region, but it is a good starting point for the rest of our algorithm.

The segmentation of the myocardium is described in Jolly *et al.* [11]. The polar space transformation is fairly straightforward, its center and maximum radius are calculated from the blood pool estimates. Then, the goal of the gray scale analysis (illustrated in Fig. 1) is to build histograms for the lungs, myocardium and blood pool distributions. We use the multiseeded fuzzy connectedness approach proposed in [12]. Rough histograms for the lungs, myocardium, and blood are built using the LV blood pool estimates. The fuzzy connectedness algorithm is then seeded using the pixels in the center of the main peaks in those histograms. It groups pixels into homogeneous regions from which the final histograms are built.

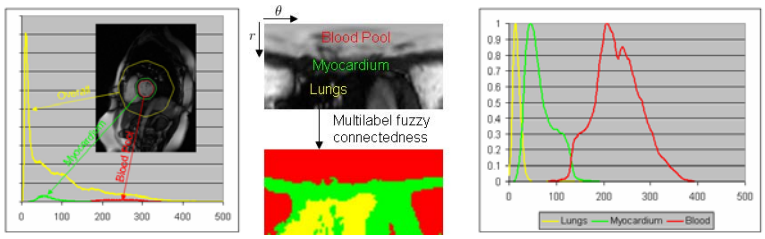

(a) (b) (c)

Fig. 1. Gray level analysis: (a) Original histograms; (b) Polar image and multiseeded fuzzy connectedness region labeling; (c) Final histograms.

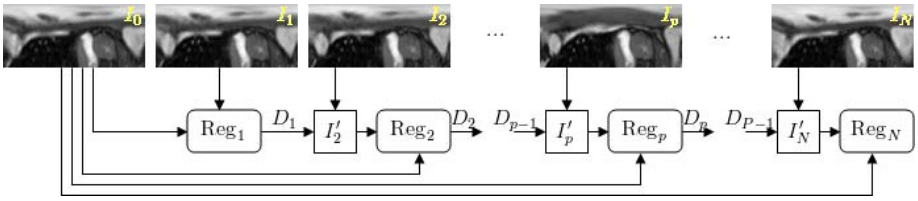

Fig. 2. Strategy to capture the large deformations between pairs of phases (especially ED and ES) during registration in polar space.

We choose the first slice to be segmented as the first slice on which an LV blood pool was detected. It is usually a clean slice, below the valve plane, without many papillary muscles inside the blood pool. It is a good candidate to start the segmentation process which will be described shortly. For the other slices, the segmentation of the first slice is propagated in both directions to the apex and to the base by applying deformable registration [13] to align the ED and ES phases of the current slice to the previous slice. The resulting deformed contours define shape priors.

To segment a given slice, we first register all the phases in the slice using a variational non-rigid algorithm [13] and generate an average image. The registration algorithm is applied to the polar images because the contours will be recovered in polar space and the intrinsic motion of the myocardium is mostly radial. To overcome the fact that there might be a large deformation between frames (especially between ED and ES), the registration from one frame to the reference frame is initialized with the registration from the previous frame to the reference frame as illustrated in Fig. 2.

The endocardium and epicardium contours are recovered independently in the average image using a shortest path algorithm. Since it is very difficult to design the best cost function that will work in all possible cases, we have chosen to generate multiple contour candidates as illustrated in Fig. 3. First, the phases are aligned separately to the ED and ES phases to produce the average images $I_{ED}(x)$ and $I_{ES}(x)$. Then, we compute two different class probabilities: a) the distribution probability $\mathcal{P}^H(x)$ is the response of the class histogram to the pixels in the average image, for the lungs ($\mathcal{P}^H_L(x)$), blood ($\mathcal{P}^H_B(x)$) and myocardium ($\mathcal{P}^H_M(x)$); b) the label probability $\mathcal{P}^L(x)$ is the average of the label images $\mathcal{L}_p(x)$ produced by the multiseeded fuzzy connectedness algorithm for the lungs, blood and myocardium. The gradi-

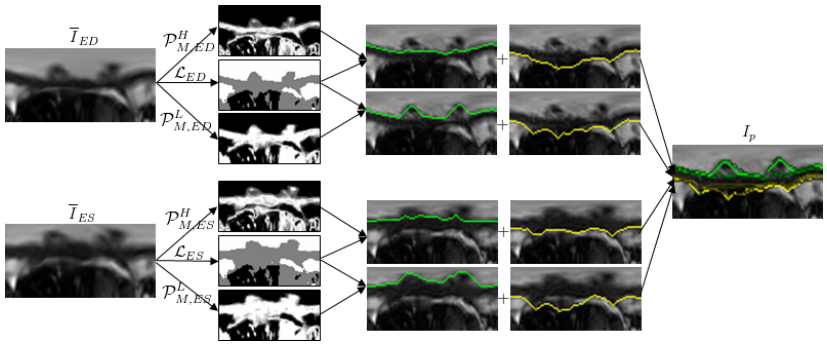

Fig. 3. Segmentation of the average images to generate multiple candidate contours.

ent cost function for each type of probability image is computed by combining the gradients of the probability images, of the original image, and of the label image.

The endocardium cost function is defined as:

$$G_k^{\text{endo}}(x) = \frac{1}{\{\frac{g(\mathcal{P}_M^i,x)+0.25g(\mathcal{L}_k,x)}{1.25}\}^2 + \epsilon},\ k = ED, ES,\ i = H, L \tag{1}$$

and the epicardium cost function is defined as:

$$G_k^{\text{epi}}(x) = \frac{1}{\{\frac{g(\mathcal{P}^i,x)+g(I_k,x)+0.25g(\mathcal{L}_k,x)}{2.25}\}^2 + \epsilon},\ k = ED, ES,\ i = H, L \tag{2}$$

where

$$g(\mathcal{P}^i, x) = \frac{g(\mathcal{P}_M^i, x) + g(\mathcal{P}_B^i, x) + g(\mathcal{P}_L^i, x)}{3},\ i = H, L.$$

In addition, when prior contours are available (for all but the first slice), the gradient images are combined with the distance maps from the prior contours as follows:

$$\begin{aligned} \hat{G}_k^{\text{endo}}(x) &= G_k^{\text{endo}}(x)(\tfrac{D_k^{\text{endo}}(x)}{2} + 1) \\ \hat{G}_k^{\text{epi}}(x) &= G_k^{\text{epi}}(x)(\tfrac{D_k^{\text{epi}}(x)}{2} + 1) \end{aligned} \qquad k = ED, ES.$$

We use Dijkstra's algorithm to recover the shortest path. All the pixels in the leftmost column in the polar image are initialized as starting points on the path and as soon as a path reaches a pixel in the rightmost column, the algorithm terminates. The contours generated by the shortest path algorithm using the two different probability images for the two average images are transfered back to all the phases using the corresponding deformation fields to obtain four different candidate contours per phase. These contours are then combined using a minimal surface algorithm.

The minimal surface algorithm was proposed by Grady [14] to extend the shortest path algorithm to 3D. This extension of the shortest path algorithm accepts one or more closed 2D contours as input and produces the global minimal surface, with respect to the cost function, having these 2D contours as its boundary.

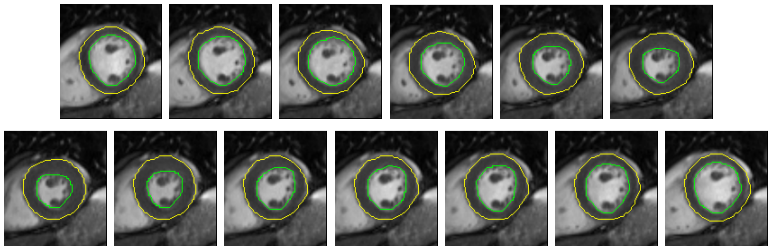

Fig. 4. Segmentation of an entire slice (cropped for better viewing).

The cost functions $G_p^{\text{endo}}(x)$ and $G_p^{\text{epi}}(x)$ for each phase p are defined in a fashion similar to Eq. (1)-(2). Then, different pixels are emphasized for the endocardium or the epicardium cost function.

The endocardium should stay behind the papillary muscles, so we emphasize pixels that are farther from the center of the candidate contours. A distance map is initialized column by column in polar space by setting to 0 the pixels on candidate contours with largest row position and good gradients. If there are no pixels with good gradient on the candidate contours for a particular column, the average prior position is set to 0. The distance map is then expanded using the traditional chamfering technique and combined with the gradient cost function to produce the final endocardium cost function.

$$\hat{G}_p^{\text{endo}}(x) = G_p^{\text{endo}}(x)\frac{D_p^{\text{endo}}(x)}{2}. \tag{3}$$

For the epicardium, more candidates have to be retained because there are many missing and spurious edges. Again, a distance map is initialized by setting pixels on candidate contours to value $D_p^{\text{epi}}(i,j) = \|i - i_0\|$ where i_0 is the average row position for the prior contours or the average thickness in the case of the first slice (when there is no prior contours). It is expanded and combined with the gradient cost function as for the endocardium (Eq. (3)).

To initialize the contours for the minimal surface algorithm, we apply Dijkstra's algorithm in the ED phase to generate a 2D contour. The 3D volume consists of all phases with the ED phase as the first phase and added again as the last phase. This way, the algorithm is initialized with two contours and the minimal surface is generated between them. In order to not bias the algorithm with the initial contour, we apply a second pass where the initial contour is the ES contour from the first pass and the 3D volume goes from the ES phase to the ES phase. Once the contours have been segmented, they are converted back to Cartesian space. Fig. 4 shows an example of the segmentation results in an entire slice.

3 Experiments

As part of the MICCAI grand challenge on left ventricle segmentation, the method was evaluated on 15 training datasets and 15 validation datasets. Our algorithm is quite fast, it takes 1 minute to segment an average dataset with 200 images (0.3 s per image) on a dual core laptop (2.33GHz and 2GB RAM). Our segmentation contours

	Detect		Good		EF (%)		LV mass (g)		Dist (mm)		Dice	
patient	endo	epi	endo	epi	auto	manual	auto	manual	endo	epi	endo	epi
SC-HF-I-01	100	100	100	100	23.65	26.16	152.96	116.75	2.63	2.06	0.88	0.93
SC-HF-I-02	100	100	100	100	22.25	25.46	133.38	141.84	2.07	1.91	0.89	0.94
SC-HF-I-04	100	100	100	100	19.03	21.82	136.78	132.08	1.72	1.94	0.93	0.94
SC-HF-I-40	100	100	100	100	34.40	40.61	104.59	87.09	1.64	1.26	0.92	0.95
SC-HF-NI-03	100	100	100	100	19.71	16.76	216.40	154.59	2.73	1.95	0.90	0.95
SC-HF-NI-04	100	100	100	100	19.88	20.37	121.63	107.84	2.25	1.51	0.91	0.95
SC-HF-NI-34	100	100	90	100	30.58	34.39	196.61	171.05	1.82	2.39	0.90	0.92
SC-HF-NI-36	100	100	100	100	16.76	15.68	167.60	113.56	1.35	2.18	0.95	0.94
SC-HYP-01	100	100	92	86	58.11	61.06	71.96	74.10	1.86	2.55	0.89	0.91
SC-HYP-03	100	100	100	100	54.78	60.54	109.58	94.38	1.79	1.48	0.90	0.94
SC-HYP-38	100	100	100	100	69.73	77.82	167.30	124.35	2.61	2.04	0.75	0.91
SC-HYP-40	100	100	72	100	31.86	44.13	98.50	85.36	3.23	2.03	0.76	0.92
SC-N-02	100	100	100	100	53.49	55.61	94.89	82.72	2.13	1.20	0.85	0.95
SC-N-03	100	100	100	100	48.28	50.31	70.59	68.97	1.38	1.53	0.92	0.94
SC-N-40	100	100	100	100	47.88	42.05	88.43	61.38	2.10	2.20	0.86	0.92

Table 1. Results on the MICCAI challenge training dataset.

were compared to the ground truth using the evaluation program. The datasets and evaluation criterion are fully described in [15]. The results are reported in Tables 1 and 2. We only report EF and LV mass for the case where the papillary muscles are included inside the cavity since our algorithm encloses them inside the endocardium and does not produce separate contours.

Fig. 5 shows the regression and Bland-Altman plots for the EF and LV mass measurements. For the EF, the slope is not quite 1, demonstrating a bias (-5.22 on the Bland-Altman plot). However, the regression coefficient is very good, and the spread of the values is pretty low. For the LV mass, it can be seen that the regression coefficient is lower (mostly due to the outlier: SC-HYP-08), the bias is larger (18.38). Therefore, the algorithm is pretty accurate at computing the EF, but not as accurate for the LV mass.

The raw results are summarized in Table 3. It can be seen that the contours are always detected and they are good (less than 5 mm from the ground truth) on the average 95% of the time for the endocardium and 97% of the time for the epicardium. This means that the contours are very satifactory and do not need to be edited much. This is in agreement with the visual examination, where 7 of the segmentations were considered excellent and only 4 were poor. No segmentation was deemed unusable making this method ready for clinical use. The average error is $2\frac{1}{4}$ mm for the endocardium and just under 2 mm for the epicardium. As suggested by the expert examiner, we will focus our effort on improving the accuracy of the segmentation around the outflow tract.

4 Conclusions

We have proposed a fully automatic system to segment the left ventricle myocardium from cine MR images. The method combines automatic localization through Fourier

	Detect		Good		EF (%)		LV mass (g)		Dist (mm)		Dice		Visual
patient	endo	epi	endo	epi	auto	manual	auto	manual	endo	epi	endo	epi	exam
SC-HF-I-05	100	100	100	100	28.51	33.03	148.56	115.45	1.36	1.59	0.94	0.96	3
SC-HF-I-06	100	100	100	100	19.89	25.78	170.17	147.34	1.74	1.60	0.93	0.95	1
SC-HF-I-07	100	100	88	100	29.07	28.18	139.33	114.12	3.02	1.89	0.85	0.95	1
SC-HF-I-08	100	100	100	100	19.76	21.42	187.01	124.40	3.07	2.17	0.87	0.93	3
SC-HF-NI-07	100	100	96	92	19.26	12.91	182.85	130.54	3.68	1.60	0.84	0.95	3
SC-HF-NI-11	100	100	100	100	13.76	14.84	195.81	158.25	2.21	1.95	0.91	0.94	1
SC-HF-NI-31	100	100	100	100	30.26	35.59	157.39	127.38	2.13	1.93	0.91	0.93	1
SC-HF-NI-33	100	100	100	90	46.12	58.35	137.62	130.78	2.32	3.22	0.87	0.94	1
SC-HYP-06	100	100	92	100	49.18	60.43	116.27	91.59	2.38	3.29	0.87	0.93	1
SC-HYP-07	100	100	94	100	55.68	62.27	192.61	133.55	2.68	2.28	0.84	0.90	3
SC-HYP-08	100	100	89	80	44.57	58.69	240.43	278.17	3.16	2.14	0.86	0.91	2
SC-HYP-37	100	100	62	86	58.06	71.68	92.60	125.38	1.83	1.28	0.90	0.93	1
SC-N-05	100	100	100	100	48.83	62.81	74.47	73.50	1.99	1.81	0.87	0.91	2
SC-N-06	100	100	100	86	47.67	54.59	83.66	64.02	2.21	1.49	0.87	0.95	2
SC-N-07	100	100	94	100	38.14	59.06	109.54	102.34	2.77	2.57	0.85	0.92	2

Table 2. Results on the MICCAI challenge validation dataset.

	Detect		Good		Dist (mm)		Dice		Visual
	endo	epi	endo	epi	endo	epi	endo	epi	exam
min	100	100	62	80	1.35	1.20	0.75	0.90	1
max	100	100	100	100	3.68	3.29	0.95	0.96	3
average	100	100	95.62	97.29	2.26	1.97	0.88	0.93	1.8
std dev	0	0	8.83	5.76	0.59	0.48	0.04	0.02	-

Table 3. Summarized results over all 30 datasets (15 validation datasets for the visual examination).

analysis and isoperimetric clustering, and segmentation through deformable registration, shortest paths, and minimal surfaces. We demonstrated on 30 datasets from the MICCAI challenge that the results look very good and the errors are small enough that the system can be used in clinical settings.

References

1. Lorenzo-Valdés, M., Sanchez-Ortiz, G., Elkington, A., Mohiaddin, R., Rueckert, D.: Segmentation of 4D cardiac MR images using a probabilistic atlas and the EM algorithm. Medical Image Analysis **8** (2004)
2. Jolly, M.: Automatic segmentation of the left ventricle in cardiac MR and CT images. International Journal of Computer Vision **70**(2) (2006)
3. Mitchell, S., Lelieveldt, B., van der Geest, R., Bosch, H., Reiber, J., Sonka, M.: Multistage hybrid active appearance model matching: Segmentation of the left and right ventricles in cardiac MR images. IEEE Trans. Medical Imaging **20**(5) (2001)
4. Fradkin, M., Ciofolo, C., Mory, B., Hautvast, G., Breeuwer, M.: Comprehensive segmentation of cine cardiac mr images. In: MICCAI. (2008)

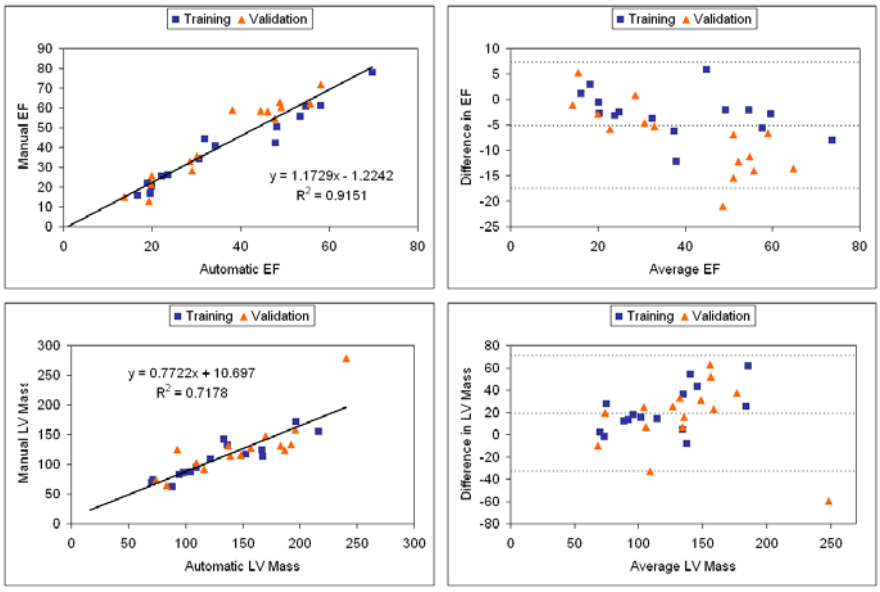

Fig. 5. Regression curve and Bland-Altman plot for the ejection fraction and left ventricle mass.

5. Lynch, M., Ghita, O., Whelan, P.F.: Segmentation of the left ventricle of the heart in 3-D+t MRI data using an optimized nonrigid temporal model. IEEE Trans. Medical Imaging **27**(2) (2008)
6. Sun, W., Çetin, M., Chan, R., Willsky, A.: Segmentation of the evolving left ventricle by learning the dynamics. In: ISBI. (2008)
7. Paragios, N.: A level set approach for shape-driven segmentation and tracking of the left ventricle. IEEE Trans. Medical Imaging **22**(6) (2003)
8. Lorenzo-Valdés, M., Sanchez-Ortiz, G., Mohiaddin, R., Rueckert, D.: Atlas-based segmentation and tracking of 3D cardiac MR images using non-rigid registration. In: MICCAI. (2002)
9. Jolly, M.P.: Automatic recovery of the left ventricular blood pool in cardiac cine MR images. In: MICCAI. (2008)
10. Grady, L., Schwartz, E.L.: Isoperimetric partitioning: A new algorithm for graph partitioning. SIAM Journal on Scientific Computing **27**(6) (2006) 1844–1866
11. Jolly, M.P., Xue, H., Grady, L., Guehring, J.: Combining registration and minimum surfaces for the segmentation of the left ventricle in cardiac cine MR images. In: MICCAI. (2009)
12. Jolly, M.P., Grady, L.: 3D general lesion segmentation in CT. In: ISBI. (2008)
13. Hermosillo, G., Chefd'hotel, C., Faugeras, O.: Variational methods for multimodal image matching. International Journal of Computer Vision **50**(3) (2002)
14. Grady, L.: Computing extact discrete minimal surfaces: Extending and solving the shortest path problem in 3D with application to segmentation. In: CVPR. (2006)
15. Radau, P., Lu, Y., Connelly, K., Paul, G., Dick, A.J., Wright, G.A.: Evaluation framework for algorithms segmenting short axis cardiac MRI. The MIDAS Journal - Cardiac MR Left Ventricle Segmentation Challenge (2009)